Electrostatic Charging and Radiation Shielding Design Philosophy for a Synchronous Satellite

W. R. Elkman,* E. M. Brown,† D. V. Z. Wadsworth,‡ E. C. Smith,§ and P. F. Adams¶
Hughes Aircraft Company, El Segundo, California

The dielectric surfaces of a spacecraft exposed to the Earth's magnetospheric plasma and trapped electron environment build up differential voltages which can result in electrostatic discharges in surface materials. These discharges result in transient ground currents and radiated electromagnetic energy which can degrade the function of electronics units and thermal control surfaces. In addition, the Earth's trapped electron and proton radiation environment causes optical and mechanical damage to surface materials and degradation of active semiconductor device performance. This paper describes an approach to reducing the hazards of these phenomena by discussing the radiation hardness design of a specific communications satellite. The methods used to identify design weak points, test materials, and develop new materials are described. Specific implemented materials and design practices which have reduced the susceptibility of the spacecraft to surface charging and radiation damage effects are noted.

Introduction

THIS paper is organized so that the total dose hardening method is presented first, followed by the electrostatic charging design. The total dose hardening methodology is well established, while the charging design approach is continuing to evolve. The charging design consists of sections concerning materials categorization, resistivity requirements, NASCAP modeling, lumped element modeling, and material charging tests.

Radiation Hardening for Total Dose

The ionizing dose deposited by the trapped radiation environment in semiconductors causes changes in the device parameters which were determined by radiation tests. Shielding analyses were performed to determine an upper bound magnitude of the mission dose that each part will receive so that the part performance degradation could be factored into the design of the circuits. The analyses and tests performed to harden the satellite system to meet lifetime requirements are summarized in the flow chart in Fig. 1.

The radiation environment is specified contractually. The source of the environment is either from the literature[1] or derived for nongeosynchronous orbits from the standard models with the programs ORB[2] and ORP.[3] The elements of the orbit are input to ORB, which writes a data set of the point by point particle trapping parameters B and L. The data set is read by ORP, which then interpolates in data sets representing the model environment and outputs the daily integral spectrum of electrons and protons.

Dose depth curves for two simple geometries, a semi-infinite slab and a solid sphere, are then calculated with the program SHIELDOSE,[4] which incorporates the results of Monte Carlo calculations for electron transport and bremsstrahlung production and transport. The curves in Fig. 2 represent the dose at the center of a slab with twice the shield thickness indicated and the dose at the center of a solid sphere with a radius equal to the shield thickness for an environment for a geosynchronous orbit. The solid sphere dose is approximately a factor of 3 greater than the dose for slab geometry. These curves are used for rough estimates of doses and shielding effectiveness.

Sector shield analyses are used to obtain mass distributions for the actual space vehicle geometry. The significant structures of the spacecraft are modeled in a modified version of the computer program MEVDP,[5] and mass distribution around selected points is determined for approximately 1000 rays. The solid sphere depth-dose curve is used to determine the contribution of each ray to the total dose. The complexity of the box models is varied as the design matures. There are three levels of analyses used in dose assessment.

Level I: Doses are calculated for a typical empty box at various equipment locations with no other boxes present.

Level II: Doses at representative points are determined for an empty box of the correct dimensions. All the other boxes are included as solids with correct average density.

Level III: The empty box is filled with all relevant internal shields and doses at critical piece parts calculated.

In the early phases of the design, only a Level I analysis is feasible. Dose contour maps were issued to the circuit designers for preliminary hardness assessment.

Circuit analyses are based on part parameter degradation obtained from radiation test data. A handbook compiling data obtained on previous programs was issued to the designers. All potentially susceptible new parts were tested in a Cobalt 60 source to obtain radiation performance characteristics. A screen based on the initial Level I analysis eliminated many circuits and units from further consideration. Figure 3 shows dose contours for a Level I analysis.

As the system design matured, a Level II analysis was performed and doses determined for boxes remaining after the initial screen. The circuit analyses were reviewed and fixes were incorporated. The options available included changing operating bias on transistors (thereby increasing power demands), substitution of another part, and shielding.

If shielding was indicated as a "fix," a Level III analysis was performed. If the dose in critical parts was still too large,

Presented as Paper 82-0116 at the AIAA 20th Aerospace Sciences Meeting, Orlando, Fla., Jan. 11-14, 1982; submitted Jan. 22, 1982; revision received Jan. 20, 1983.

*Staff Physicist, Math and Physics Department, Technology Division.
†Section Head, Vehicle Integration Department, Technology Division.
‡Senior Staff Physicist, Malibu Research Laboratories.
§Senior Scientist, Math and Physics Department, Technology Division.
¶Senior Staff Physicist, Math and Physics Department, Technology Division.

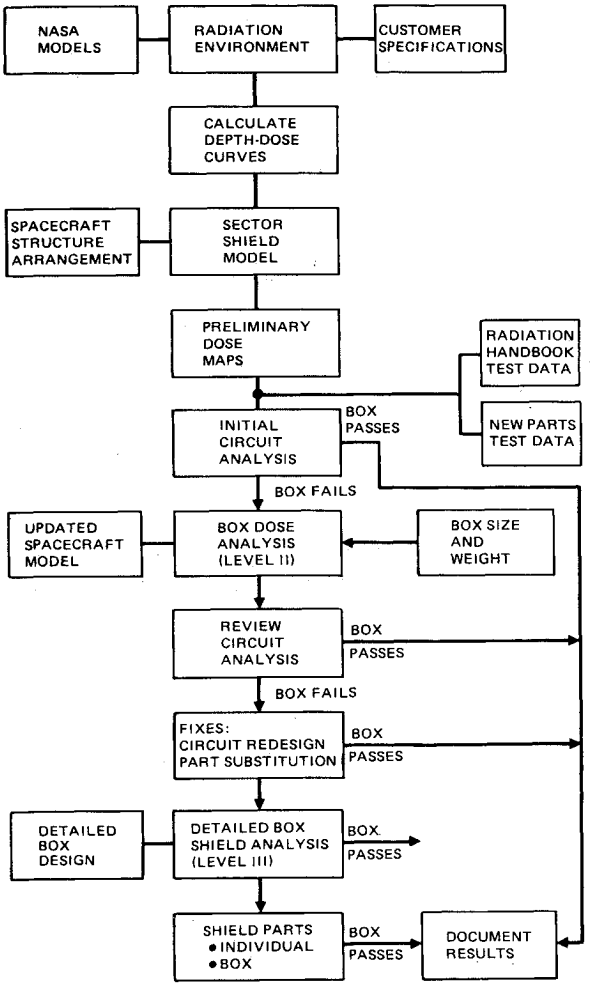

Fig. 1 Flow of design implementation for radiation hardening.

the effects of various shield configurations were assessed. The product designer made a weight trade study of local piece part shields, increased thickness of box walls or covers, and local patch shields. By a combination of shield analysis, circuit design and analysis, and shield implementation, a system design which meets mission lifetime requirements was achieved.

Electrostatic Charging Design

The selection of spacecraft exterior surfaces is restricted by a rigid set of thermal-radiative properties. The spacecraft design incorporates a passive thermal control approach, which radiates the heat from internal sources and reflects solar radiation in order to maintain the payload at temperatures necessary to meet mission life requirements. The physical size and weight restrictions imposed by launch vehicle payload capacity and the need to provide adequate surface area for the solar cells for electrical power production limit the area available for thermal control. The spacecraft design, therefore, requires the use of a small class of dielectric thermal control materials which possess low solar absorptance, high infrared emittance, light weight, and mechanical, chemical, and radiation stability over a wide temperature range and under ultraviolet and charged particle irradiation.

Communications satellites, typical of early 1970 designs, had minimal charging control measures, and did experience some on-orbit anomalies. Three important materials—second surface quartz and Teflon mirrors and Kapton thermal blankets—were believed to have been degraded by discharge effects or to have acted as arc discharge sources.

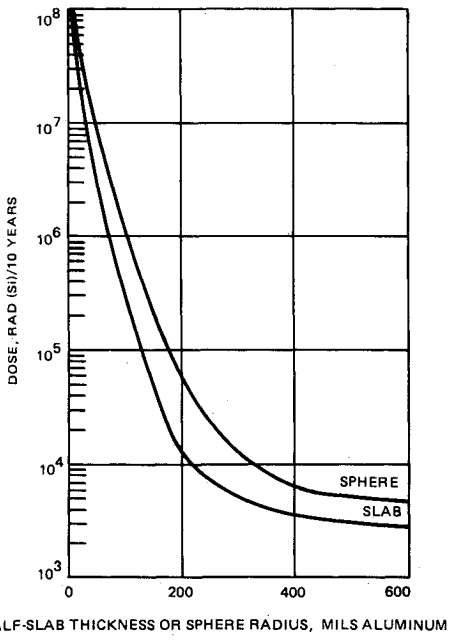

Fig. 2 Dose vs shielding; 10-yr geosynchronous orbit.

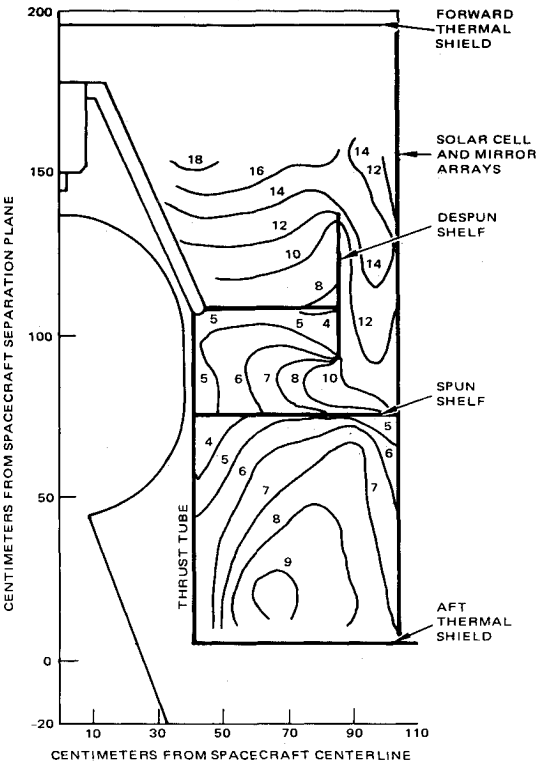

Fig. 3 Isodose contours (in milliradians).

For the spacecraft under consideration here, a variety of analytical and test methods were used to estimate the effects of the plasma substorm environment. The surface materials subject to exposure to the space plasma charging environment were identified. The material compositions, shapes, locations, charging characteristics, and electrical grounding paths were categorized. Results of electrical charging and resistance tests for these materials were noted. Requirements for grounding individual surfaces were specified. The need was established for requirements and for material charging tests which had not been developed. Surface areas which were considered sensitive to charging included antennas, forward and aft thermal barriers, forward and aft solar cell arrays, optical

solar reflectors, and the apogee motor nozzle. Figure 4 shows the calculation sequence for the electrostatic charging design.

A series of material development programs, supplemented by applications to present technology and related scientific investigations, were performed. Specific materials which have been evaluated are edge-coated quartz mirrors, perforated Kapton and Teflon, germanium coated Kapton, a laminate of aluminum mesh on Kapton, various epoxy and polyurethane paints, and a conductive coating for Kevlar composites.

The charging control design of the spacecraft was established based on these investigations and considerations of other studies. The edge-coated mirrors are located on the solar cell array drum exterior, where the reduction of charging effects is aided by photoemission. The extendable solar panel forms a large shaded cavity, which is coated with the conductive spray developed for coating on Kevlar composite. The forward thermal barrier and antenna blankets are protected by a combination of painted aluminum foil, germanium coated Kapton, perforated Teflon, and bonded mesh on Kapton, depending on the required thermal properties.

The specific analytical and test methods used will be discussed in the following sections. The analytical methods consist of categorization of charging properties, resistivity requirements, a NASCAP analysis, and a lumped element analysis. Electron beam and insulation resistance measurements comprise the test section.

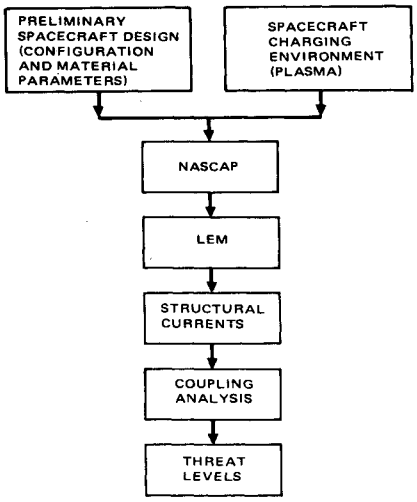

Fig. 4 Sequence of calculations for ESD threat level determination.

Analytical Methods to Define Charging Potentials and Hazards from Discharge

Categorization of Charging Properties of Surface Materials

A study was made of the composition, shape, charging characteristics, and grounding methods of surface materials after the spacecraft design was established. Figure 5 illustrates the spacecraft configuration. Table 1 shows the materials which were characterized.

Development of Resistivity Requirements

The categorization of materials isolated the portions of the spacecraft structure sensitive to the effects of charging. Conservative or worst-case calculations to estimate surface and bulk voltage gradients were used.

It is assumed in the calculations that equilibrium exists, and the current balance to the spacecraft is determined by the charging characteristics of all the exterior surfaces and their paths to ground. There is no net current to the spacecraft overall, but there are sources and sinks of current to specific surfaces. The extent of these sources and sinks is partly determined by geometry, view factors for solar irradiation and photoemission, secondary emission, bulk and surface resistivity, and material capacitance. For worst-case analyses, secondary emission is disregarded and photoemission is in-

Table 1 Material data for dielectrics

Material	Treatment	Maximum surface voltage, kV	Arc energy, mJ
0.002 VDA Teflon	None	8	150
	ITO	0.2-0.5	No arcs
0.002 VDA Kapton	None	14	160
	⅜-in. spacing pinholes	...	Arcs under 20-kV beam only
	⅜-in. hexagonal Al grid	7	1
	⅜-in. conductive paint grid	5-10	No arcs
	ITO		No arcs
0.002 Teflon/aluminum foil laminate	None	8	124
	⅜-in. spacing pinholes	8.5	193
	⅛-in. spacing pinholes	4.5	35
	⅜-in. hexagonal Al grid	8	2
0.005 Teflon/aluminum foil laminate	0.48 square grid	9.2	200
	0.24	8.9	25
0.008 quartz mirrors	None	4	16
	Edge coated	9.5	Arcs under 2-nA/cm^2 beam only
	ITO (clear conductive coated)	0.2	No arcs
0.0035 Kevlar on aluminum honeycomb core	Acetylene black filler in resin	Minimal	10^6-10^9 Ω/square
	None	7.9	5.7×10^{13} Ω-cm^2
0.2-μm Ge film on 0.002 VDA Kapton (with isolated VDA grids)	None		8.7×10^9 Ω/square
Paint	Chemglaze white A-276	0.8	
	CTL-15 gloss black		1.3×10^7 Ω-cm

cluded by assuming that photocurrent neutralizes the plasma current for some materials.

In addition, the plasma current magnitude is often considered independent of the surface coordinates (and the view factors neglected). However, careful attention is made to the effects of surface geometry and parallel resistive paths on surface voltage using magnetostatic forms of Maxwell's equations (Poisson's equation). In this manner, a conservative assumption is made that each surface charges to a voltage given by the product of the plasma current and the material resistivity. For this spacecraft, a resistivity requirement was established for each of the surfaces in Table 1.

NASCAP Modeling

A NASCAP analysis was used to model the large-scale charging behavior of the spacecraft.[6] Figure 6 shows the potential contour plot for the illuminated case. The analysis indicated that the most negative surface voltage in the unilluminated case, corresponding to eclipse, reached −3900 V, and ranged between −2160 and 0 V for the illuminated case. These results indicate that in both instances voltages relative to spacecraft ground may not be low enough to reduce the risk of arcing to acceptable levels (as determined by comparison to arcing threshold levels estimated from ground tests).

A single Maxwellian electron and ion charge distribution was used to simulate the plasma substorm charging environment. The electron and ion temperatures were 10 kV, and the corresponding particle densities were 1 particle/cm^3. The charging simulation was performed with and without 1 sun intensity solar illumination at an angle of 23 deg to the spacecraft axis normal. The illuminated case analysis was made for a nonspinning spacecraft because the vehicle contains both a spun and despun section, a situation

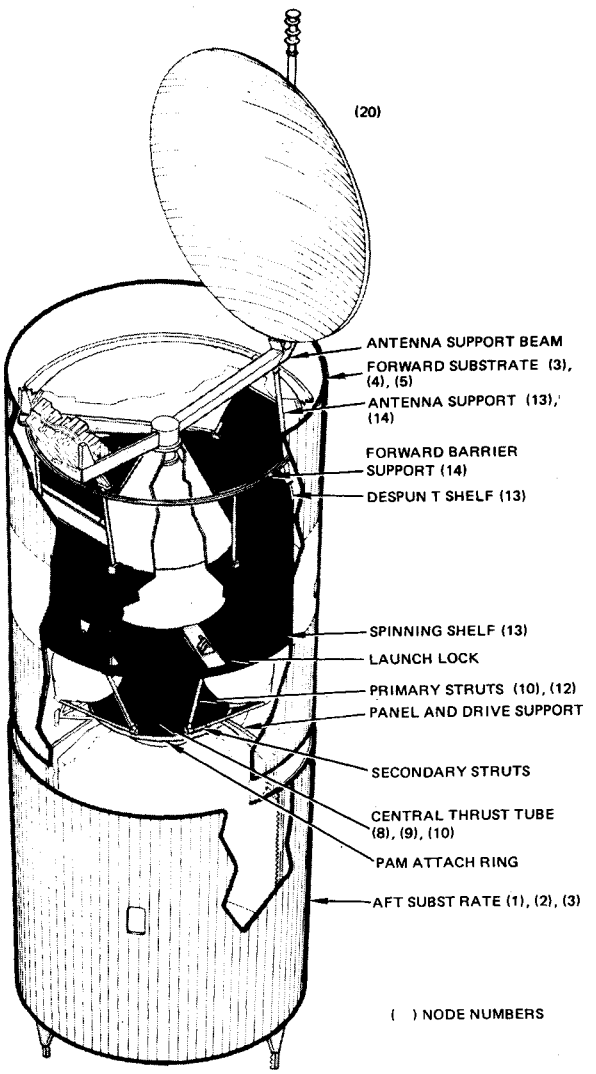

Fig. 5 Spacecraft structure assembled view.

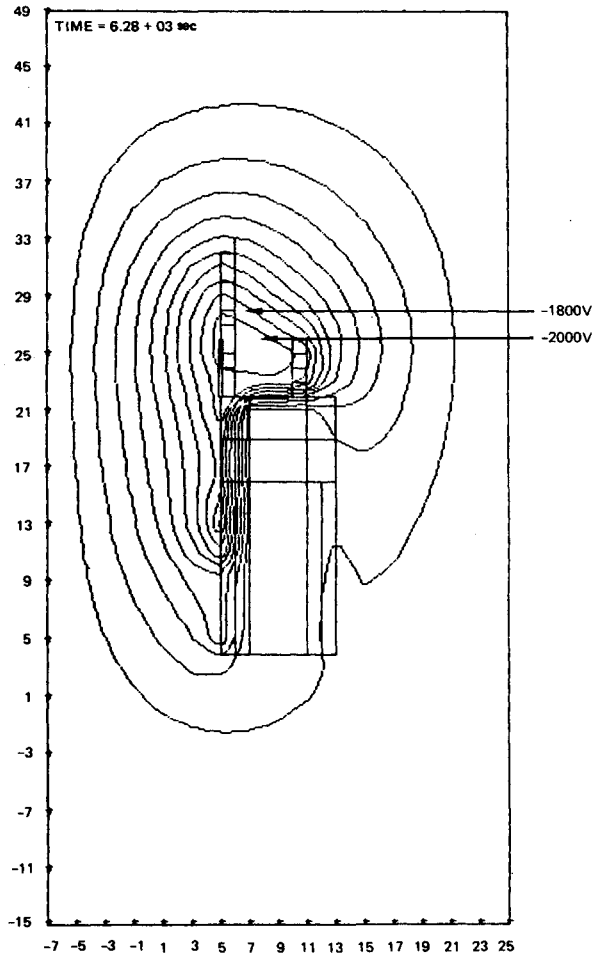

Fig. 6 Voltage contour plot for illuminated condition charged in a 10-kV plasma.

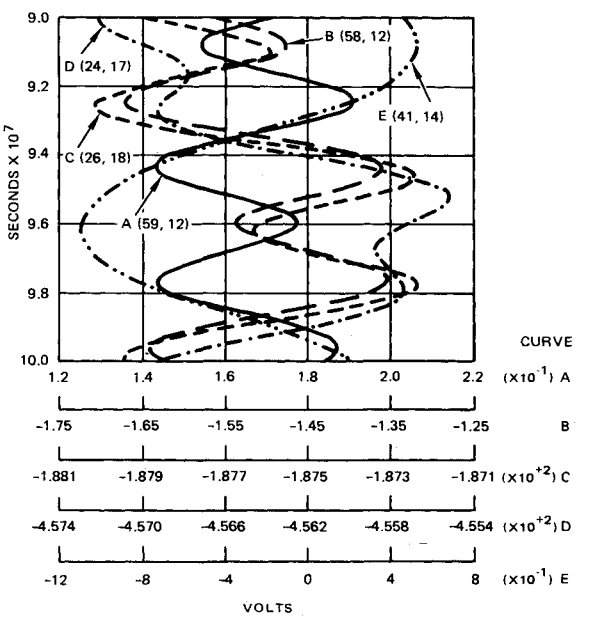

Fig. 7 Voltage plots across sensitive nodes.

NASCAP cannot simulate properly. The despun case is presumed to simulate the worst-case charging environment for an illuminated spacecraft.

The spacecraft surface materials were modeled in moderate detail. This included quartz solar cell and optical solar reflector covers, white nonconductive paint on the forward thermal barrier, black conductive paint on the inner facesheet of the aft solar array cavity, Kapton antenna reflector surfaces, and Kapton boom surfaces.

Lumped Element Model

A lumped element circuit model analysis and cable coupling analysis were performed to specify locations of hazardous transient currents due to electrostatic discharge. Surface material voltage thresholds for arcing were obtained from available test data. These levels were compared to surface voltages estimated from surface charging calculations to identify surface materials likely to arc. Energy and frequency content of postulated arcs were estimated from test data and used to formulate current sources for the lumped element circuit model. The coupling of structural currents to cables was calculated. It was estimated that currents of several tens of amperes are possible on the spun and despun shelves, resulting in cable currents of up to several amperes.

In order for the lumped element treatment to make sense, it is considered necessary that the largest circuit element dimensions be smaller than the smallest wavelengths used in the analysis. A major part of the modeling involved the calculation of inductances, capacitances, and radiation resistances.

The model was constructed from tabulation of material types, geometry, and interconnections between structural elements. The bulk and surface resistivities to ground and capacitances to infinity of these materials were categorized to determine the surface charge buildup level of the satellite. The interior materials surface resistivity, inductance, coupling capacitance, and joint resistance were classified to calculate the interior current distribution due to surface arcs.

The electrostatic charging behavior of the spacecraft surface materials was determined from the literature and from tests.[7,8] The energy of arcs was tabulated from test data for solar cell covers, Kevlar substrates, VDA Teflon with pinholes, and Kapton with hexagonal metal mesh. The arc duration was estimated from Refs. 9 and 10. These current pulses were used as sources in the lumped element circuit

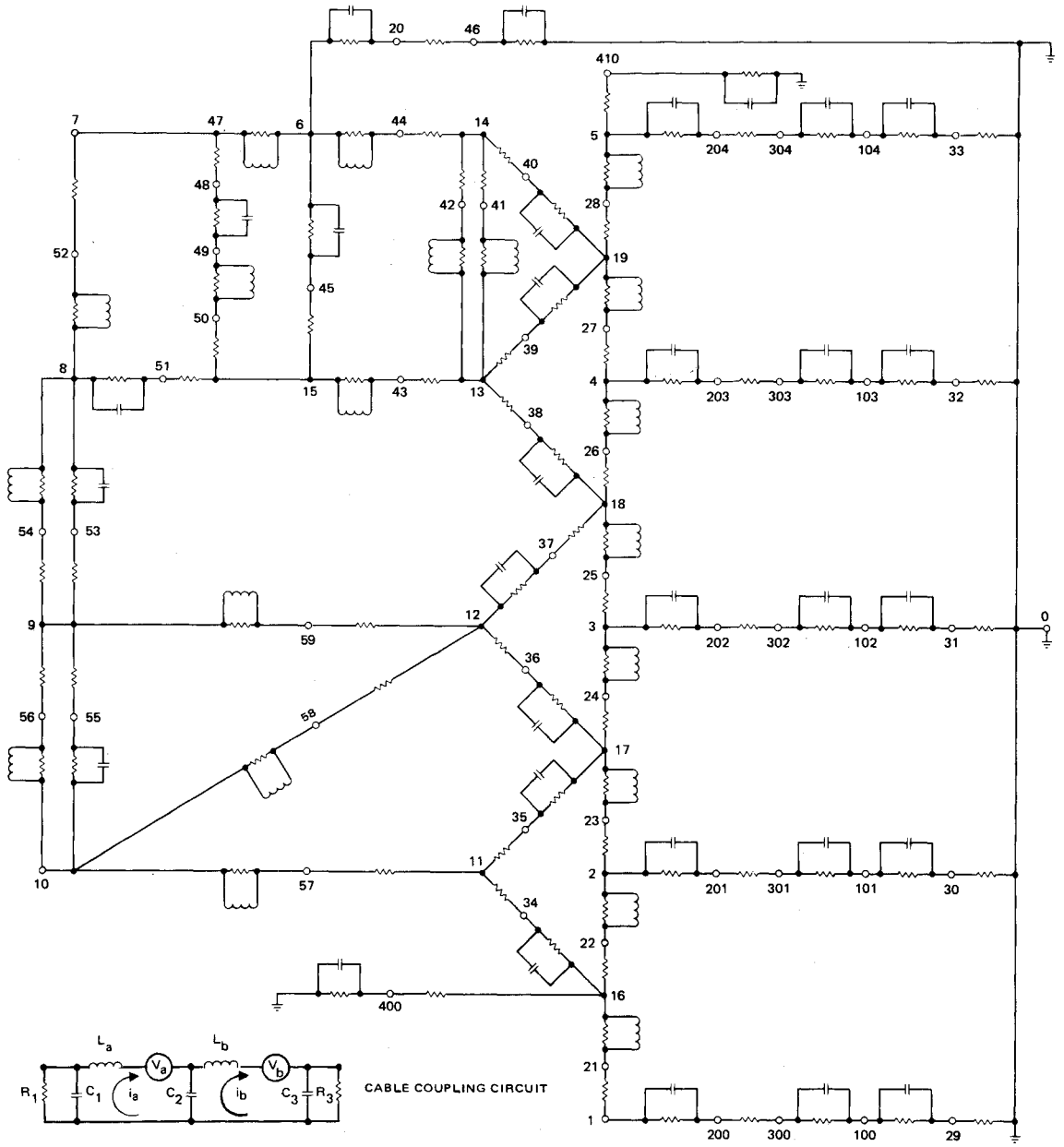

Fig. 8 Lumped element circuit model (circumferential elements not modeled).

Table 2 Circuit element values and method of computation

Circuit element and type	Evaluation method	Value	Electrical formula
Solar array total, capacitance	Capacitance to infinity as prolate spheroid a = 1/2 (86 in. +78 in.), b = 1/2 (83.5 in.)	154 pF	$4\pi\epsilon_o(a^2-b^2)^{1/2}\left(\tanh^{-1}(1-b^2a^{-2})^{1/2}\right)^{-1}$ (6) a, b semi major and minor axis
Segmented solar array to provide source nodes; both inductance and capacitance; both radial and circumferential	Geometric apportionment of C's, L's obtained treating spheroid as waveguide to infinity		$V_p^2 = \frac{\ell^2}{LC}$, L and C related by phase velocity
Circumferential		(0.538, 3.09, 4.55, 6.53, 4.54 pF) for 8 segments	$C_C = \frac{C_\infty}{\pi d}\frac{\Delta w}{w}$, $\Delta w/w$ is fraction spheroid height (heights of 0.116, 0.664, 0.977, 1.403, 0.975 meters)
			L_C's computed from C_C's
Longitudinal (axial)		(14.3, 2.49, 1.69, 1.18, 1.70 μH)	$C_\ell = C_\infty\frac{\Delta h}{h}\frac{\Delta w}{w}$, here $\Delta h/h$ is length and and $\Delta w/w$ is width fraction (lengths are same as circumferential heights so C's are same)
		(0.552, 2.62, 2.05, 4.66 μH) Note inductances start at nodes	L_ℓ's computed from C's
Superstructure, capacitance	Capacitance to infinity as disc, r = 36 in.	64.7 pF	$8\epsilon r$
Despun shelf, inductance circumferential and radial	Annulus treated as unwrapped strip with width 1/2 (OD - ID) = 16.5 in., length π/2(OD + ID) = 157 in.		
Circumferential 8 elements in parallel parts		1.39 μH each	$2\ell\left(\frac{\mu_o}{4\pi}\right)\left[\ell n\left(\frac{2\ell}{t+w}\right)+\frac{1}{2}+0.2235\left(\frac{t+w}{\ell}\right)\right]$ (7)
Radial, 4 elements		0.089 μH each	with $t \ll w$
Spun structure struts, inductance (8 struts) from thrust cylinder to spun shelf)	Long cylinder (1.05 in. diameter, 25 in. long, 0.028 in. B_e wall)	0.50 μH each	$L = \frac{2\mu_c\mu_o\ell}{4\pi}\ell n\left(\frac{\ell}{a}\right)$ (8)
Thrust tube cylinder, self-inductance (2 vertical cylinders topped by spun cone coaxial with despun cone)	Hollow cylinders (lower, 17 in. radius, 28 in. length) (Middle, 16 in. radius, 13 in. length)	0.14 μH 0.042 μH	$L = 2\delta\left(\frac{\mu}{4\mu}\right)\left[\frac{h}{\delta}\ell n\left(\frac{h}{\delta}+\sqrt{\left(\frac{h}{\delta}\right)^2+1}\right)-\sqrt{\left(\frac{h}{\delta}\right)^2+1}+1\right]$ (9)
Internal self-inductance used here speculative	(Upper spun average radius 10.3 in., 18 in. length)	0.05 μH	$L_i = \frac{1}{\sigma\delta}\frac{1}{2\pi r}\frac{\sinh(2d/\delta)-\sin(2d/\delta)}{\cosh(2d/\delta)-\cos(2d/\delta)}$ (10)
Internal and external speculatively used	(Upper despun cone same shape)	0.12 μH	$L_i = L_i + \frac{\ell\mu_o}{2}\ell n\frac{2\ell}{r} - 1$ (11)
Forward thermal barrier, inductance (radial and circumferential)	(Unwrapped) strip into 4 segments with ℓ = 34 in. W_{avg} = π68 in. for radial and ℓ_{avg} = π68 in., w = 34 in. for circumferential	0.52 μH each radial 0.83 μH each circumferential	$L = 2\ell\left(\frac{\mu_o}{4\pi}\right)\left[\ell n\left(\frac{2}{t+w}\right)+\frac{1}{2}+0.2235\left(\frac{t+w}{\ell}\right)\right]$ (12)
Aft thermal barrier radial inductance (circumferential not evaluated	(Unwrapped) to strips into 8 segments w = π/2 (81 in. +21 in.), ℓ = (81 in. - 21 in.)/2	0.87 μH each	(12)
Capacitance			
Forward barrier to reflector	Approximate coupling between discs of diameters 68 in. and 72 in.	17.5 pf	$C = k\left(\frac{\epsilon_o}{d}\right)\sqrt{S_1S_2}$ (13) k~1, d is separation between surfaces of approximate areas S_1 and S_2. (13)
Forward barrier to despun shelf	Approximate coupling between annulus (66.5 in., 33.5 in. dia.) and disc 76 in.	24.5 pf	
Solar array to thrust tube	Approximate coupling between concentric cylinders of 33.7 in. height, 81 in. and 34.5 in. dia.	55.8 pf	$\frac{C}{\ell} = \frac{2\pi\epsilon}{\ell n(b/a)}$ (14)
Thrust tube to despun shelf	Ignored by comparison to spun/despun cone coupling		
Despun shelf to solar array inner facesheet (upper and lower)	Approximate coupling of 31.4 in. high, 81 in. dia. cylinder by 41 in. centroid separation to annulus (for lower 11.8 in. high cylinder)	25.0 pf (upper) 15.3 pf (lower)	(13) (13)

Table 2 (continued)

Circuit element and type	Evaluation method	Value	Electrical formula
Aft barrier to thrust tube and spun shelf to thrust tube	Left out because electrically continuous region		
Aft barrier to solar array (upper and lower)	Coupling of 33.7 in. high cylinder to annulus (81 in., 37.in. dia.) (upper); annulus to 78 in. high cylinder (lower)	30.3 pf (upper) 35.9 pf (lower)	(13)
Facesheet capacitance of solar array substrate (honeycomb core to solder cell backing)	Parallel plane surfaces 0.0035 in. separation	99.6 nf/m^2	$\frac{C}{m^2} = \frac{\epsilon}{t}$ (15)
Solar cell cover to cell surface capacitance (deposited charge surface to cell collection fingers)	Parallel plane surfaces, 0.012 in. separation	29 nf/m^2	(15)
Cell surface to solder backing capacitance	Parallel plane surfaces, 0.011 in. separation	32 nf/m^2	(15)
Forward barrier to solar array	Approximate coupling 41.1 in. centroid separation; 31.4 in. high, 81 in. dia. cylinder to 76 in. disc	32.9 pf	(13)
Spun to despun shelves	Approximate coupling of two annular surfaces separated by 11.8 in.	63.5 pf	(13)
Spun shelf to solar array (upper and lower array)	Approximate coupling of annulus (80.5 in., 32 in. dia.) to 11.8 in. high array segment by 41 in. separation	19.7 pf	(13)
Spun shelf to aft barrier	Approximate coupling to annular regions by 33.7 in. separation	27.9 pf	(13)
Radiation and Default Resistances			
Space vehicle exterior longitudinal resistance	Exterior surface treated by equating S/V length to 1/2 wavelength (86 in. + 78 in. + 72 in.)	95 ohms	Dipole radiator
Segmentation of S/V exterior value into parallel and series strips	Segment heights of 9.1, 31.4, 11.8, 33.7, 39 in.	3.7, 17., 4.8, 13.6 and 15.8 ohms	Geometric segmentation of single S/V element
Circumferential exterior values disregarded for simplified model but used on later S/V	Small loop antenna expression with the circumference treated as 1/2 the wavelength		$R_{rad} = 20\pi^2\left(\frac{2\pi a}{\lambda}\right)^4$ ohms (16)
Struts from spun shelf to thrust cylinder	8 struts treated as small dipoles	2.2 ohm each	$R_{rad} = 80\pi^2\left(\frac{h}{\lambda}\right)^2$ (17)
Thrust cylinder	Treated as small dipoles of 28 in., 13 in. and 18 in.	2.8, 0.60 and 1.1 ohms	(17)(Approximate because h/λ should be small)
Defaults for series and parallel elements		0.1 ohm series and 10^6 ohm shunt	

model. The circuit equations were then solved, using the SPICE2 computer program. Figure 7 shows the time dependence of voltages across sensitive nodes. Figure 8 shows the lumped element model, and Table 2 shows the circuit element expressions.

A simplified analysis of the inductive coupling of structural currents to electrical cables was made. The current coupling from structure to cables is computed by estimating the loop size formed by structure and cable. The structure current is used to compute the magnetic field. This field is used to compute the voltage induced in the loop. The voltage is treated as a source for the loop, and cable termination impedances are included in the loop equations. The resulting equations were solved parametrically. The induced current extends from 0.5 to 5.0 A at 30 MHz for typical cable dimensions and termination impedances.

Electron Beam Charging Tests and Insulation Resistance Measurements

Charging tests of the surface materials were performed. Flat samples of flight configuration surface materials were irradiated with a monoenergetic or multienergetic electron beam to determine the sample charging and arcing characteristics. In some circumstances, high-resistance ohmmeter measurements were made to aid in selecting surface materials. The results of these tests are shown in Table 1.

The charging simulation test setup has been described in Ref. 7. Several improvements to the facility have been made. A multienergetic capability has been added to the electron source to more accurately represent a double-Maxwellian distribution function. A repetitive 10-s-period, linear ramp is used to drive the electron beam high voltage power supply. The beam energy and current density are varied linearly between 0 and 15 KeV and 0 and 2 nA/cm^2 to obtain a 1 nA/cm^2 time-averaged current density. The maximum voltage capability has been increased to 30 kV, and the maximum current density to 45 nA/cm^2. A closed loop controller for the filament cathode of the electron source has been installed to maintain beam current density. A microcomputer-based data acquisition system has been installed to record back current, wall current, Faraday-cup current, and sample surface voltage at a user-selectable time interval.

The charging and arcing behavior of materials tested in the simulation chamber are categorized by calculating the effective resistivity, highest surface voltage, and arc energy and frequency. The resistivity at a specific beam voltage is estimated by forming the ratio of the equilibrium surface voltage to the sample return current (to ground). This is compared to the results of insulation resistance tests. The arc energy is estimated by the change in capacitive energy of a sample before and after arcing. The capacitance is ordinarily estimated from the value for a parallel plane capacitor filled with the dielectric material being tested.

Insulation resistance measurements were performed on materials which were candidates for use on spacecraft exterior surfaces to determine if a charging hazard existed.

A method for making contact probe surface and bulk resistivity measurements was devised that conforms to the ASTM D257-76 standard for insulation resistance measurements.[11] Three potential probes are used in the measurement: a negative potential probe, a positive return probe, and a guard probe (maintained at the negative probe potential). The resistance is measured using a high-resistance ohmmeter (capable of impressing up to 1000 V) which incorporates a guard circuit to shunt extraneous parallel surface currents from the measuring circuit. For bulk resistivity measurements, the flat central negative probe is placed on the facesheet to be measured, surrounded by an annular guard probe. The positive return probe is attached to the rear surface of the sample. Appropriate allowances are made for the long charging times required for highly resistive and capacitive samples.

Conclusion

The methods for total dose shielding and reduction of electrostatic charging effects described in this paper have been applied to an existing spacecraft. The satisfactory on-orbit performance of this spacecraft indicates the total dose methodology is adequate, while additional improvement in the charging design is warranted.

References

[1]Stassinopolous, E.G., "The Geostationary Radiation Environment," *Journal of Spacecraft and Rockets,* Vol. 17, March-April 1980, p. 145.

[2]Teague, M.J. and Viette, J.I., "A Model of the Trapped Electron Population for Solar Minimum," Report NSSDC 74-03, NASA Goddard Space Flight Center, Greenbelt, Md., April 1974.

[3]Teague, M.J., and Viette, J.I., "The Use of the Inner Zone Electron Model AE-5 and Associated Computer Programs," Report NSSDC 72-11, NASA Goddard Space Flight Center, Greenbelt, Md., Nov. 1972.

[4]Selzer, S.M., "Electron-Bremsstrahlung and Proton Depth-Dose Data for Space Shielding Applications," *IEEE Transactions on Nuclear Science,* Vol. NS-26, Dec. 1979, p. 4896.

[5]Liley, B. and Hamilton, S.C., "Modified Elemental Volume Dose Program (EVDP)," AFWL-TR-69-68, Air Force Weapons Laboratory, Kirkland AFB, N. Mex., May 1968.

[6]Cassidy, J.J., "NASCAP User's Manual," SSS-R-78-3739, Sytems, Science and Software, La Jolla, Calif., Aug. 1978.

[7]Robinson, P.A. Jr., "The Behavior of Partially Metallized Kapton for Spacecraft Charging Control," *Journal of Spacecraft and Rockets,* Vol. 16, March 1979, p. 104.

[8]Stevens, N.J. et al., "Testing of Typical Spacecraft Materials in a Simulated Substorm Environment," *Proceedings of the Spacecraft Charging Technology Conference,* 1977, Air Force Geophysics Laboratory, Hanscom AFB, Mass., p. 431; see also, NASA TMX-73537, 1977.

[9]Balmain, K.C., Cuchanski, M., and Kromer, P.C., "Surface Micro-Discharges on Spacecraft Dielectrics," *Proceedings of the Spacecraft Charging Technology Conference,* p. 519; see also, NASA TMX-73537, 1977.

[10]Ling, D., "Common Approach to Solving SGEMP, DEMP, and ESD Survivability," *Proceedings of the Spacecraft Charging Technology Conference,* p. 789; see also, NASA TMX-73537, 1977.

[11]"Standard Test Methods for DC Resistance or Conductance of Insulating Materials," D257-76, American Society for Testing and Materials, Philadelphia, Pa., 1976.